Inorganic Chemistry

ARTICLE

pubs.acs.org/IC

Dissection of the Mechanism of Manganese Porphyrin-Catalyzed Chlorine Dioxide Generation

Thomas P. Umile, Dong Wang, and John T. Groves*

Department of Chemistry, Princeton University, Princeton, New Jersey 08544, United States

Supporting Information

ABSTRACT: Chlorine dioxide, an industrially important biocide and bleach, is produced rapidly and efficiently from chlorite ion in the presence of water-soluble, manganese porphyrins and porphyrazines at neutral pH under mild conditions. The electron-deficient manganese(III) tetra-(*N*,*N*-dimethyl)imidazolium porphyrin (MnTDMImP), tetra-(*N*,*N*-dimethyl)benzimidazolium (MnTDMBImP) porphyrin, and manganese(III) tetra-*N*-methyl-2,3-pyridinoporphyrazine (MnTM23PyPz) were found to be the most efficient catalysts for this process. The more typical manganese tetra-4-*N*-methylpyridiumporphyrin (Mn-4-TMPyP) was much less effective. Rates for the best catalysts were in the range of 0.24−32 TO/s with MnTM23PyPz being the fastest. The kinetics of reactions of the various ClO_x species (e.g., chlorite ion, hypochlorous acid, and chlorine dioxide) with authentic oxomanganese(IV) and dioxomanganese(V)MnTDMImP intermediates were studied by stopped-flow spectroscopy. Rate-limiting oxidation of the manganese(III) catalyst by chlorite ion via oxygen atom transfer is proposed to afford a *trans*-dioxomanganese(V) intermediate. Both *trans*-dioxomanganese(V)TDMImP and oxoaqua-manganese(IV)TDMImP oxidize chlorite ion by 1-electron, generating the product chlorine dioxide with bimolecular rate constants of 6.30×10^3 M^{-1} s^{-1} and 3.13×10^3 M^{-1} s^{-1}, respectively, at pH 6.8. Chlorine dioxide was able to oxidize manganese(III)TDMImP to oxomanganese(IV) at a similar rate, establishing a redox steady-state equilibrium under turnover conditions. Hypochlorous acid (HOCl) produced during turnover was found to rapidly and reversibly react with manganese(III)TDMImP to give dioxoMn(V)TDMImP and chloride ion. The measured equilibrium constant for this reaction (K_{eq} = 2.2 at pH 5.1) afforded a value for the oxoMn(V)/Mn(III) redox couple under catalytic conditions (E' = 1.35 V vs NHE). In subsequent processes, chlorine dioxide reacts with both oxomanganese(V) and oxomanganese(IV)TDMImP to afford chlorate ion. Kinetic simulations of the proposed mechanism using experimentally measured rate constants were in agreement with observed chlorine dioxide growth and decay curves, measured chlorate yields, and the oxoMn(IV)/Mn(III) redox potential (1.03 V vs NHE). This acid-free catalysis could form the basis for a new process to make ClO_2.

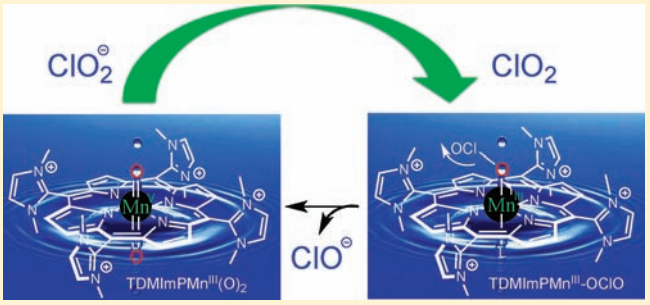

INTRODUCTION

Chlorine dioxide has emerged as the preferred agent for microbial decontamination, for wood pulp bleaching and for the detoxification of sites contaminated by biological warfare agents such as anthrax.[1,2] As a broad-spectrum biocide, chlorine dioxide has advantages over chlorine because of its higher potency against bacteria, viruses, and parasites while having a decreased tendency to produce haloacetic acids and chloroform. Both gaseous and aqueous solutions of chlorine dioxide, sometimes in concert with paraformaldehyde, have proven to be effective in the decontamination of *Bacillus anthracis* spores in buildings and on machinery.[3] Despite these advantages, the commercial production of chlorine dioxide (ClO_2) continues to be problematic because of its instability for long-term storage. Industrial processes to produce ClO_2 typically involve the oxidation of chlorite ion[2] or the reduction of chlorate ion[4] using strong acids and/or oxidizing/reducing agents leading to inventory storage issues and complications arising from inconsistent product purity.[1] In particular, contaminants in the product stream such as chlorine and chlorate ion can cause corrosion of equipment or toxicity concerns.[2,5] Moreover, the instability of ClO_2 mandates that all of these process issues be addressed directly at the point-of-use. Clearly, there is a need for a simpler, more reliable[6] and more green process[7] for the production of ClO_2.

Recently, we reported the discovery that ClO_2 can be produced rapidly and efficiently using a highly electron-deficient, water-soluble manganese porphyrin catalyst.[8] Key advantages of this system are the mildly acidic to neutral reaction conditions, full conversion of the chlorite starting material, high activity on a solid support, and the fact that ClO_2 production occurred within seconds. A more typical cationic manganese porphyrin has been reported to give significantly slower rates and incomplete conversion.[9] For both of these manganese porphyrin systems, the production of ClO_2 contrasts markedly from the oxygen-producing

Received: July 6, 2011
Published: September 21, 2011

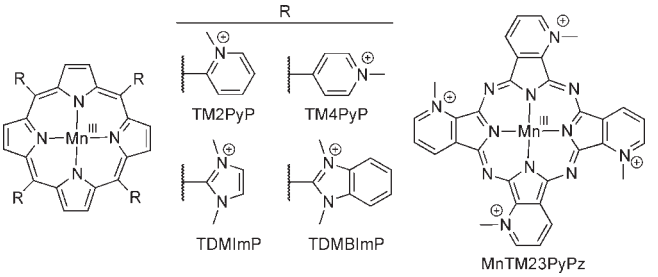

Figure 1. Manganese porphyrins and porphyrazine studied as catalysts.

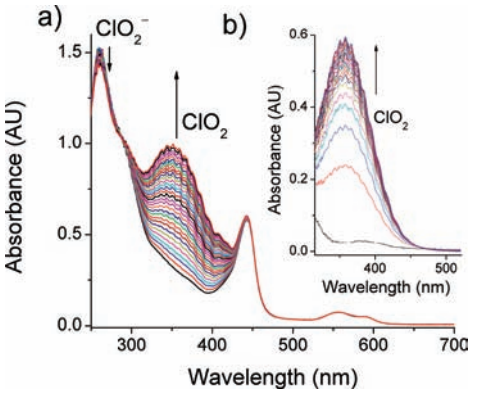

Figure 2. (a) Rapid appearance of ClO_2 (359 nm) from the MnTDMImP-catalyzed disproportionation of ClO_2^- (10 mM) at pH 6.8 with 0.1 mol % catalyst (445 nm) showing the first 30 s of reaction, 1 scan/s. (b) Similar reaction with MnTM23PyPz (9 mM sodium chlorite, 10 μM MnTM23PyPz, pH 4.7 100 mM acetate buffer) showing the first 30 s of reaction, 1 scan/s.

pathway catalyzed by the heme protein chlorite dismutase[10] and synthetic iron porphyrins.[11]

Here we describe a dissection of the mechanism of chlorite ion oxidation to ClO_2 catalyzed by this active manganese tetra-(*N*,*N*-dimethyl imidazolium) porphyrin (MnTDMImP). The goals of this effort were to determine which properties of the manganese complex are essential for effective catalysis and to elucidate which of several likely pathways are involved. The well-characterized oxoMn^{IV} and *trans*-dioxoMn^{V} oxidation states of this particular porphyrin[12−14] have facilitated the direct observation of each individual step in this catalysis. In addition we describe remarkably high catalytic activity for chlorine dioxide production by a cationic manganese porphyrazine.

RESULTS

Catalytic Generation of ClO_2 from ClO_2^-. Several cationic, water-soluble manganese porphyrins and a similar porphyrazine complex catalyzed the rapid production of chlorine dioxide from chlorite ion under mild conditions (Figure 1). The evolved ClO_2 could be monitored from the appearance of the characteristic chromophore at 359 nm (Figure 2).[15] During turnover, the visible spectra of the Mn^{III} catalysts remained largely unchanged, demonstrating the resistance of the catalyst to bleaching as well as providing mechanistic insight (vide infra). The initial turnover rates for each of the studied catalysts are reported in Table 1. Extremely high activity (32 TO/s) was observed for the manganese(III) porphyrazine, MnTM23PyPz.

Table 1. Turnover Frequencies of ClO_2 Generation

	initial turnover	
catalyst	frequency (s^{-1})	mol % cat.
MnTM4PyP[a]	0.01	0.25
MnTM2PyP[a]	0.24	0.25
MnTDMImP[a]	0.40	0.25
MnTDMBImP[a]	0.48	0.50
MnTM23PyPz[b]	32.0	0.27

[a] pH 6.8 50 mM phosphate buffer, T = 25 °C, 2.0 mM $NaClO_2$. [b] pH 4.5 50 mM acetate buffer, T = 25 °C, 1.8 mM $NaClO_2$.

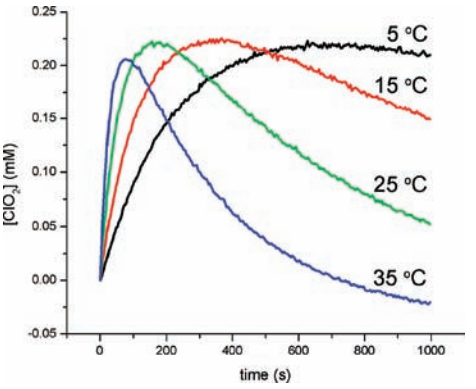

Figure 3. Effect of temperature on the evolution of ClO_2 upon mixing 2.0 mM ClO_2^- and 10 μM Mn^{III}TDMImP. ClO_2 concentration is measured by the change in absorbance at 359 nm. Subtle changes in the catalyst spectrum at this wavelength over very long reaction times resulted in an overestimate of ClO_2 decay at 35 °C. Experimental conditions: 100 mM pH 6.8 phosphate buffer.

The appearance of ClO_2 using MnTDMImP was studied in 100 mM acetate buffer (pH 4.7 and 5.7) and 100 mM phosphate buffer (pH 6.8). Initial turnover frequencies observed under these conditions at 25 °C for 2 mM ClO_2^- and 10 μM Mn^{III}TDMImP were 1.00, 1.03, and 0.42 at pH 4.7, 5.7, and 6.8, respectively. However, the turnover frequency was influenced more by buffer composition than by pH. Increasing buffer concentration and ionic strength (with added sodium perchlorate) was found to inhibit the MnTDMImP-catalyzed reaction by a factor of 5 in the range 5 mM−100 mM (Supporting Information, Figure S1) while at a constant buffer concentration, the turnover frequency did not change from pH 5.9 to 7.01 (Supporting Information, Figure S2).

When ClO_2^- was rapidly mixed with Mn^{III}TDMImP at 25 °C, the spectroscopically observed concentration of ClO_2 produced rose quickly and reached a plateau within 3 min. The product ClO_2 absorbance subsequently decayed in a slower process over the course of about 15 min. The maximum ClO_2 concentration was not affected by temperature (Figure 3), although the reaction rate increased markedly from 5 to 35 °C (Supporting Information, Figure S3).

Reduction of oxoMn^{V} and oxoMn^{IV}TDMImP by ClO_2^-. The reactions of both oxoMn^{V}TDMImP and oxoMn^{IV}TDMImP with ClO_2^- were studied by double-mixing, stopped-flow spectroscopy. In the first push, authentic oxoMn^{V} or oxoMn^{IV} was generated by mixing Mn^{III}TDMImP with 1 equiv of oxone or tBuOOH, respectively, in 10 mM pH 8.0 phosphate buffer.[12−14]

dx.doi.org/10.1021/ic201430v |*Inorg. Chem.* 2011, 50, 10353–10362

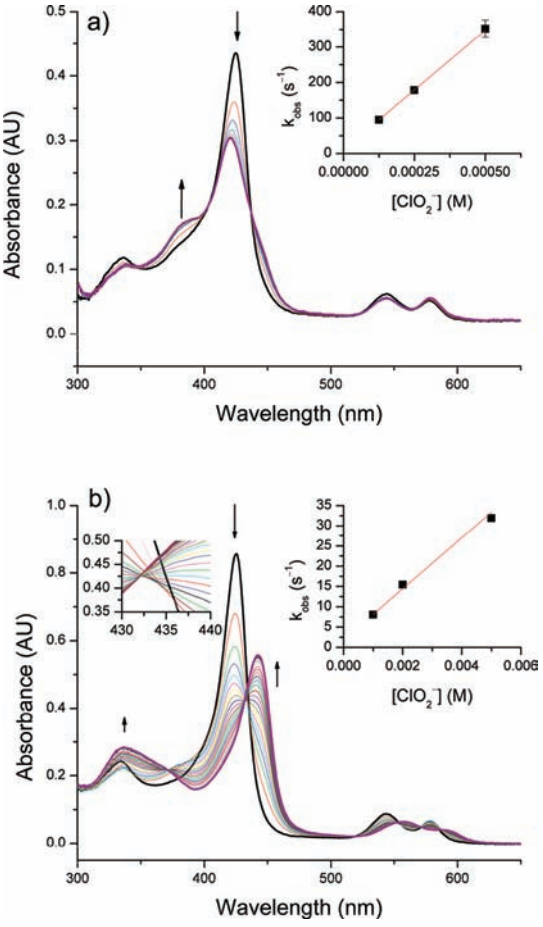

Figure 4. (a) Time-resolved UV−vis spectra of the reaction between 5 μM oxoMn^{V}TDMImP and 125 μM ClO_2^- in 100 mM pH 4.7 acetate buffer over 0.3 s. A single isosbestic point was observed at 437 nm. Inset: Plot of pseudo-first order rate constant (k_{obs}) of the decay of oxoMn^{V} versus initial $[ClO_2^-]$. The apparent second-order rate constant (k_{app}) is $(6.77 \pm 0.08) \times 10^5$ M^{-1} s^{-1}; (b) Time-resolved spectra of the reaction between 10 μM oxoMn^{V}TDMImP and 1.0 mM ClO_2^- in 100 mM pH 6.8 phosphate buffer over 3 s. Two, time-separated isosbestic points were observed, first at 436 nm (0−225 ms) and then at 432 nm (225 ms − 3.0 s). Inset: Plot of pseudo-first order rate constant (k_{obs}) of the decay of oxoMn^{V} during the first phase of reaction versus initial $[ClO_2^-]$. The apparent second-order rate constant (k_{app}) is $(6.30 \pm 0.62) \times 10^3$ M^{-1} s^{-1}. Self-decay of Mn^{V} and Mn^{IV} to Mn^{III} results in nonzero intercepts.

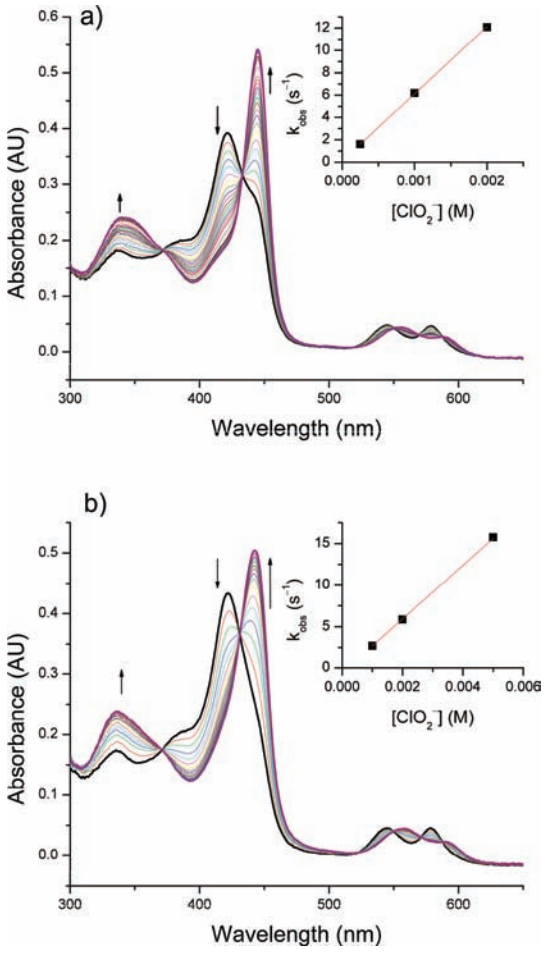

Figure 5. (a) Time-resolved UV−vis spectra of the reaction between 10 μM oxoMn^{IV}TDMImP and 1.0 M ClO_2^- in 100 mM pH 4.7 acetate buffer over 3 s. A single isosbestic point is observed at 433 nm. Inset: Plot of pseudo-first order rate constant (k_{obs}) of the decay of oxoMn^{IV} versus initial $[ClO_2^-]$. The apparent second-order rate constant (k_{app}) is $(6.03 \pm 0.06) \times 10^3$ M^{-1} s^{-1}. (b) Time-resolved UV−vis spectra of the reaction between 10 μM oxoMn^{IV}TDMImP and 1.0 M ClO_2^- in 100 mM pH 6.8 phosphate buffer over 1.5 s. A single isosbestic point is observed at 431 nm. Inset: Plot of pseudo-first order rate constant (k_{obs}) of the decay of oxoMn^{IV} versus initial $[ClO_2^-]$. The apparent second-order rate constant (k_{app}) is $(3.13 \pm 0.12) \times 10^3$ M^{-1} s^{-1}.

In the second push, oxoMn^{V} or oxoMn^{IV} was mixed with an excess of ClO_2^- in 100 mM pH 4.7 acetate or pH 6.8 phosphate buffer. This "pH jump" experiment permitted observation of the reaction between each of the high-valent manganese species with ClO_2^- at lower pH values.

The decay of oxoMn^{V} (as measured by the characteristic Soret absorbance at 425 nm[13]) was pH dependent and followed pseudo-first order kinetics when mixed with an excess of ClO_2^-. This decay was fitted to a modeled exponential decay curve to obtain the observed pseudo-first order rate constant (k_{obs}), which was plotted as a function of $[ClO_2^-]$. The apparent second-order rate constants (k_{app}) calculated from the slope of k_{obs} vs $[ClO_2^-]$ are 6.8×10^5 and 6.3×10^3 M^{-1} s^{-1} at pH 4.7 and 6.8, respectively.

At pH 4.7, the 1-electron reduction of oxoMn^{V} by ClO_2^- was fast and allowed the direct observation of the reduced oxoMn^{IV} TDMImP catalyst (Figure 4, panel a) with a single isosbestic point between the Soret bands at 437 nm. By contrast, at pH 6.8 the reaction of oxoMn^{V} with ClO_2^- afforded Mn^{III} (Figure 4, panel b). The presence of two time-separated isosbestic points (436 and 432 nm) during this reaction demonstrated the intermediacy of oxoMn^{IV} in the reaction between oxoMn^{V} and ClO_2^-. Under these conditions, the apparent second-order rate constant k_{app} was determined by first obtaining a pseudo-first order rate constant (k_{obs}) during the first phase of the reaction (where only the 436 nm isosbestic was observed).

The reaction between oxoMn^{IV} and an excess of ClO_2^- was similarly found to result in a pseudo-first order decay of oxoMn^{IV} to Mn^{III} (as measured by the characteristic Soret absorbance of oxoMn^{IV} at 422 nm) at pH 4.7 and 6.8 (Figure 5). A single isosbestic point was observed at 433 nm between the Soret bands of oxoMn^{IV} and Mn^{III}. The apparent second-order rate constants measured for the reduction of oxoMn^{IV} by ClO_2^- are 6.0×10^3 and 3.1×10^3 M^{-1} s^{-1} at pH 4.7 and 6.8, respectively.

dx.doi.org/10.1021/ic201430v |*Inorg. Chem.* 2011, 50, 10353–10362

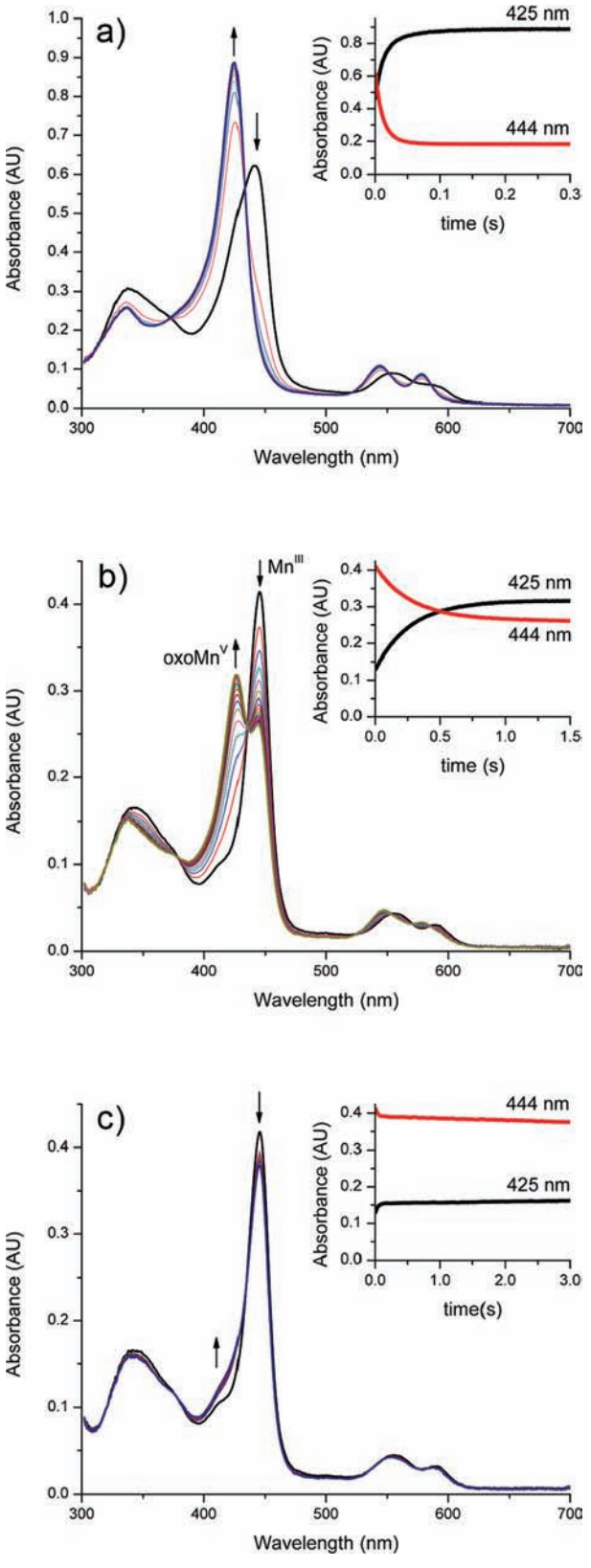

Figure 6. UV−vis spectral changes for the reaction of Mn^{III}TDMImP with HOCl at (a) pH 6.8, (b) 5.1, and (c) 4.7. Buffer conditions: pH 6.8, 100 mM phosphate buffer; pH 4.7 and 5.1, 100 mM acetate buffer. Reaction conditions: (a) 10 μM Mn^{III}, 5 equiv of HOCl; (b) 5 μM Mn^{III}, 20 equiv of HOCl; (c) 5 μM Mn^{III}, 50 equiv of HOCl.

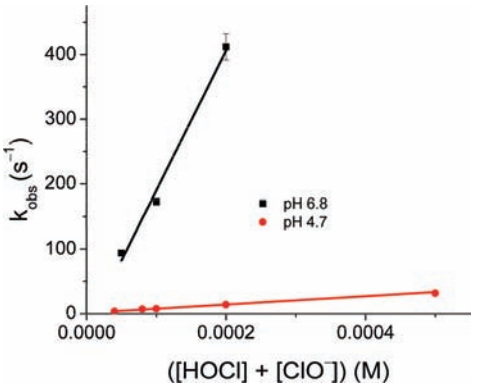

Figure 7. Determination of the apparent second-order rate constant of oxo-transfer from HOCl to Mn^{III}TDMImP. The slope of each line is equal to the product of k_{app} and the concentration of Mn^{III} ($k_{app\ 4.7}$ = $(6.64 \pm 0.23) \times 10^4\ M^{-1}\ s^{-1}$, $k_{app\ 6.8}$ = $(1.71 \pm 0.27) \times 10^6\ M^{-1}\ s^{-1}$).

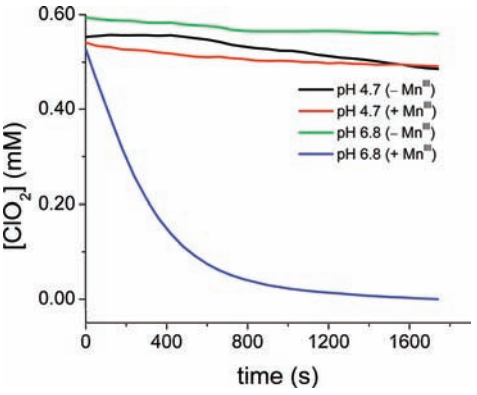

Figure 8. Comparison of the reaction of ClO_2 with 5 μM Mn^{III}TDMImP at pH 6.8 and 4.7. The ClO_2 concentration was measured at 359 nm.

Measurement of k_{app} for oxo-Transfer between HOCl and Mn^{III}. The reaction between hypochlorous acid (HOCl) and Mn^{III}TDMImP was studied by single-mixing stopped-flow spectrometry. At pH 6.8, the reaction resulted in complete formation of $oxoMn^V$ in <100 ms (Figure 6). An apparent second-order rate constant for the reaction was determined by measuring k_{obs} of $oxoMn^V$ appearance (425 nm) as a function of [HOCl] (Figure 7). The calculated rate constant (k_4) at pH 6.8 was $1.7 \times 10^6\ M^{-1}\ s^{-1}$. An initial-rate analysis of $oxoMn^V$ formation gave a slower rate constant of $1.47 \times 10^5\ M^{-1}\ s^{-1}$.

At pH 4.7, complete formation of $oxoMn^V$ could not be elicited with even a 50-fold excess of HOCl (Figure 6c). Nevertheless, the apparent second-order rate constant ($k_4 = 6.6 \times 10^4\ M^{-1}\ s^{-1}$) under these conditions was calculated from a plot of k_{obs} for the decrease in Mn^{III} absorbance (444 nm) versus [HOCl]. A similar analysis using the method of initial rates provided a lower calculated $k_4 = 4.22 \times 10^3\ M^{-1}\ s^{-1}$. After a quick reaction time (<0.1 s at pH 4.7), the concentrations of Mn^{III} and $oxoMn^V$ reached an apparent steady-state equilibrium. This steady-state observation was better demonstrated at slightly less-acidic conditions of pH 5.1.

Reaction of ClO_2 with Mn^{III}TDMImP. To account for the observed decay of ClO_2 (Figure 3), the reaction of ClO_2 with Mn^{III}TDMImP was investigated. The ClO_2 absorbance at 360 nm

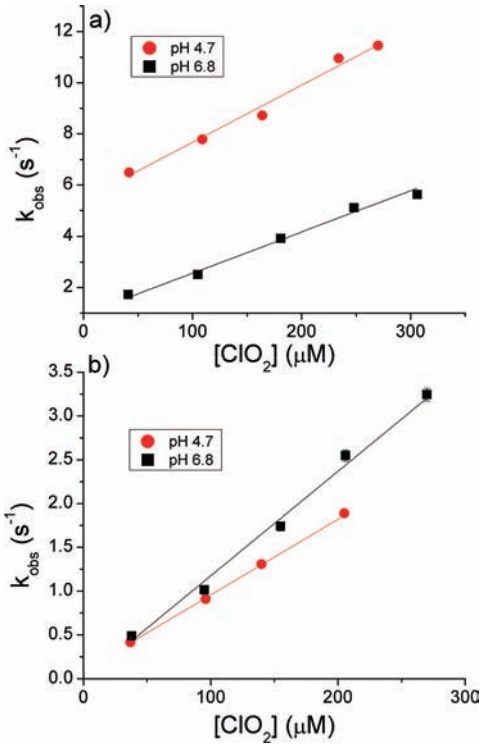

Figure 9. (a) Pseudo-first order analysis of the reaction between oxoMn^{V} and ClO_2. The observed first-order decay of oxoMn^{V} (k_{obs}) is plotted versus ClO_2 concentration. ($k_{app\ 4.7}$ = (2.24 ± 0.14) × 10^4 M^{-1} s^{-1}, $k_{app\ 6.8}$ = (1.61 ± 0.12) × 10^4 M^{-1} s^{-1}). (b) Pseudo-first order analysis of the reaction between oxoMn^{IV} and ClO_2. The observed first-order decay of oxoMn^{IV} (k_{obs}) is plotted versus ClO_2 concentration. ($k_{app\ 4.7}$ = (7.90 ± 0.53) × 10^3 M^{-1} s^{-1}, $k_{app\ 6.8}$ = (1.19 ± 0.06) × 10^4 M^{-1} s^{-1}).

quickly disappeared in the presence of Mn^{III}TDMImP at pH 6.8, but not pH 4.7 (Figure 8). In both cases, the only porphyrin oxidation state observed in solution was Mn^{III}.

Electron Transfer between oxoMn^{IV}, oxoMn^{V}, and ClO_2. Stopped-flow techniques were again used to observe how oxoMn^{V}TDMImP and oxoMn^{IV}TDMImP reacted with ClO_2. Both oxoMn^{V} and oxoMn^{IV} reacted with ClO_2 via 1-electron transfer. Although oxoMn^{IV} did not build up in the reaction of oxoMn^{V} with ClO_2, the observation of two, time-separated isosbestic points indicated the intermediacy of oxoMn^{IV} in the reaction. The product of 1-electron oxidation of ClO_2 is formally a chlorine(V) species, shown below to be chlorate (ClO_3^-). The apparent second-order rate constants (k_{app}) for the reduction of oxoMn^{V} by ClO_2 were 1.6 × 10^4 M^{-1} s^{-1} and 2.2 × 10^4 M^{-1} s^{-1} at pH 6.8 and 4.7, respectively (Figure 9, panel a). Calculated k_{app} for the reduction of oxoMn^{IV} by ClO_2 are 1.2 × 10^4 M^{-1} s^{-1} and 7.9 × 10^3 M^{-1} s^{-1} at pH 6.8 and 4.7, respectively (Figure 9, panel b).

ClO_3^- Determination by HPLC. The observation that ClO_2 itself acted as a 1-electron reductant of oxoMn^{IV}TDMImP and oxoMn^{V}TDMImP suggests that some chlorine(V) species was produced. An indirect UV-detection HPLC method[16] was therefore employed to confirm and quantify the presence of chlorate in reaction mixtures of either ClO_2^- or ClO_2 with Mn^{III}TDMImP (Table 2). Buffer, catalyst, ClO_2^-, and ClO_2 stock solutions were free of ClO_3^- prior to reaction. A measured amount of either ClO_2^- or ClO_2 was added to solutions of MnTDMImP and stirred for about 1 h before being analyzed. Because the excess buffer anions coeluted with chloride anion, the quantification of chloride produced by the catalytic decomposition of ClO_2^- could not be accomplished.

Table 2. Measured Concentrations of ClO_3^- Produced ($[ClO_3^-]_{obsd}$) from the Reaction of 10 μM Mn^{III}TDMImP with a Given Amount of Substrate (ClO_2 or ClO_2^-) at pH 6.8[a]

added substrate	$[ClO_3^-]_{obsd}$ (mM)	$[ClO_3^-]_{pred}$ (mM)
1 mM ClO_2	0.7	0.8
1 mM ClO_2^-	0.6	0.7
2 mM ClO_2^-	1.7	1.4

[a] Also shown are the ClO_3^- concentrations predicted ($[ClO_3^-]_{pred}$) by a kinetic model of the proposed mechanism (vide infra) given the same substrate/catalyst starting conditions.

Scheme 1. Proposed Mechanism for ClO_2 Evolution from ClO_2^-

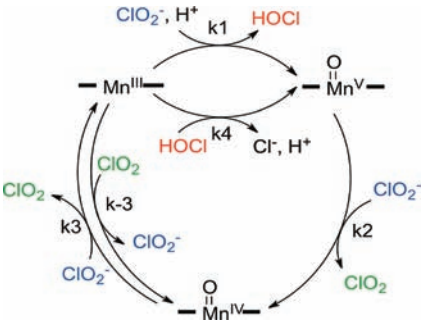

DISCUSSION

We have studied the catalytic oxidation of ClO_2^- to chlorine dioxide by water-soluble manganese porphyrins and a manganese porphyrazine. Large amounts of chlorine dioxide, representing many turnovers of the catalysts, were observed within seconds for the tetra-dimethylimidazolium porphyrin MnTDMImP, the corresponding benzimidazolium porphyrin, TDMBImP, and the cationic manganese porphyrazine MnTM23PyPz. This latter catalyst proved to react so rapidly with chlorite ion (32 TO/s) that it was difficult to analyze in detail. Those efforts are ongoing. By contrast, the reaction of chlorite ion with MnTDMImP was particularly well behaved, allowing a complete kinetic deconvolution of the primary steps in this catalysis. Given the industrial significance of ClO_2,[1,2] the need for better methods for its production, and the variety of differing known heme- and porphyrin-mediated reactions of chlorite ion,[8,10,11,17−19] it is of interest to understand the mechanisms of these reactions and to elucidate which catalyst properties favor each of these specific reactivities.

General Mechanism for Manganese Catalyzed ClO_2 Generation. We recently proposed the mechanism shown in Scheme 1 to account for the appearance of ClO_2 in these reactions.[8] The key initiating step in this catalytic cycle was suggested to be oxygen atom transfer from chlorite to the Mn^{III} catalyst to form *trans*-dioxoMn^{V}TDMImP. The thermodynamic driving force for oxo-transfer from chlorite ion is only slightly less than that of hypobromite ion (BrO^-) ($\Delta\Delta G°$ = +16.7 kJ mol^{-1}).[20] As we have reported, hypobromite is a very facile oxo-transfer agent in its reaction with Mn^{III} porphyrins,[13] with a rate constant for

dx.doi.org/10.1021/ic201430v |*Inorg. Chem.* 2011, 50, 10353–10362

Scheme 2. Reversible Reactions of Mn^{III}TDMImP with (1) HOCl and (2) ClO_2

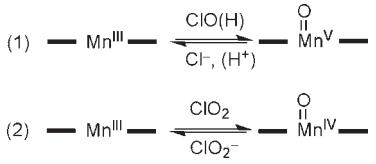

oxo-transfer from HOBr to Mn^{III}TDMImP $\sim 10^5$ M^{-1} s^{-1} at neutral pH. For the reaction with chlorite ion, the fact that the Mn^{III} oxidation state of the catalyst persisted during turnover (Figure 2) requires that any change in the porphyrin oxidation state from Mn^{III} be slow relative to Mn^{III}-forming reactions. Therefore, we conclude that the oxidation of Mn^{III} by ClO_2^- must be the rate-determining step of the overall cycle. Accordingly, a slower 2-electron oxidation of Mn^{III} by ClO_2^-, generating HOCl and *trans*-dioxoMn^V is consistent with these observations. Interestingly, the pH-independence of the turnover rate (Supporting Information, Figure S2) implies that the oxygen transfer step to afford the Mn^V species is pH independent and occurs at about the same rate as the analogous heterolysis of HOO-Mn^{III}TDMImP, which also affords Mn^V.[12]

As can be seen in the data in Table 1, higher turnover rates were observed for porphyrins with the most electron-withdrawing meso-substituents (TDMImP and TDMBImP). Although porphyrin electronics could potentially influence the binding of chlorite ion to the Mn^{III} center, porphyrin substituent effects have been shown to have little effect on the normally fast axial ligand exchange rate.[21] However, electron-withdrawing substituents on porphyrins have been shown to increase the Mn^{III}/Mn^{IV} redox potential, to stabilize *trans*-dioxomanganese(V) porphyrins by decreasing the basicity of the terminal oxo-groups, and to lower the energy of the porphyrin a_{2u} highest occupied molecular orbital (HOMO).[13,22,23] If oxidation of the manganese(III) catalyst to oxoMn^V is the rate-determining step of this reaction, the accessibility of this intermediate may be the reason the more electron-deficient porphyrins are faster catalysts.

The observed reduction of oxoMn^V and oxoMn^{IV}TDMImP by chlorite ion ($E°$ = +1.068 V)[24] to afford ClO_2 is highly analogous to the well-studied reduction of such species by nitrite ion ($E°$ = +1.04 V).[22] The similar reduction of Compounds I and II of horseradish peroxidase by chlorite ion to generate ClO_2 is also known.[18] The measured k_{app} for reduction of oxoMn^VTDMImP by chlorite ion at pH 6.8 ($6.30 \pm 0.62 \times 10^3$ M^{-1} s^{-1}) is significantly slower than those previously reported[22] for the related cationic *N*-methylpyridinium porphyrins, oxoMn^VTM4PyP and oxoMn^VTM2PyP with nitrite (1.5×10^7 and 2×10^4 M^{-1} s^{-1}, respectively) at pH 7.4. The rate of chlorite oxidation by oxoMn^VTDMImP increased by approximately 2 orders of magnitude over a $\sim$2 pH range, indicating that a single protonation of the *trans*-dioxomanganese(V) species is required for activation.[14,25]

Hypochlorous acid is proposed to be a product of the initial chlorite-Mn(III) reaction (Scheme 1). In this regard, the results for the reaction of Mn^{III}TDMImP with HOCl were very revealing. At pH 6.8, the reaction generated oxoMn^V completely within 300 ms ($k_{app\ 6.8}$ = $(2.23 \pm 0.11) \times 10^5$ M^{-1} s^{-1}) (Figure 6). However, at pH 4.7 and 5.1, Mn^{III}TDMImP and *trans*-dioxoMn^VTDMImP were apparently in *rapid, reversible equilibrium* (Scheme 2, reaction 1), similar to the behavior of bromide/hypobromite with this porphyrin.[13] The significance of this observation with respect to the proposed mechanism is that HOCl and *trans*-dioxoMn^VTDMImP are observed to be present together over the entire period of the measurement. Thus, hydrogen abstraction from H−OCl by O=Mn^V=O to afford the chloroxy radical and oxoMn^{IV} must be slow or thermodynamically unfavorable.

Table 3. Calculated Thermodynamic Parameters (K_{eq}, E) for the Reversible Oxo-Transfer from HOCl to Mn^{III}TDMImP

pH	K_{eq}	ΔE (mV)	$E_{Mn(V)/Mn(III)}$ (V, vs NHE)
4.7	$(5.1 \pm 0.5) \times 10^{-3}$	- 68 ± 1	+ (1.411 ± 0.001)
5.1	$(2.2 \pm 0.7) \times 10^{-1}$	- 20 ± 5	+ (1.352 ± 0.005)
5.6[a]	12.0	+ 32	+ 1.285

[a] ±errors represent standard deviation for multiple experiments with varying [HOCl], except for pH 5.6 where equilibrium was only observed spectroscopically for one experiment (50 μM HOCl, 5 μM MnPor).

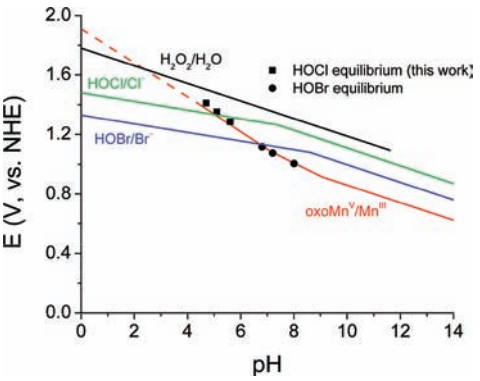

Figure 10. Plot of calculated MnTDMImP $E_{OMn(V)/Mn(III)}$ redox potential as a function of pH from HOCl equilibrium data (black squares) and HOBr equilibrium data (black circles). Nernst equation plots for HOBr/Br- (blue), HOCl/Cl- (green) and H_2O_2/H_2O (black) are superimposed for reference.

The equilibrium between HOCl/Mn^{III} and Cl^-/dioxoMn^V (Figure 6, panels b and c) allows us to directly calculate K_{eq} for the reversible oxo-transfer from dioxoMn^V to chloride ion (Scheme 2, reaction 1). This steady state could be observed at pH 4.7, 5.1, and 5.6, and the concentrations of both porphyrin species could be directly measured from the steady-state UV−vis spectrum. From these values and the known HOCl and chloride ion concentrations, an equilibrium constant K_{eq} was calculated for this oxo-transfer reaction (Table 3). This value allowed a further determination of the redox potential E(OMn^V/Mn^{III}), for oxo-transfer from oxoMn^VTDMImP. The calculated potentials as a function of pH are plotted in Figure 10.[13] As can be seen, there is a pronounced pH effect on the thermodynamics of halide oxygenation, with bromide ion oxygenation being facile at neutral pH and chloride ion oxidation becoming accessible at pH 5. The facile oxygenation of chloride ion observed here also suggests that the in situ generation of hypochlorite may be useful in other manganese porphyrin catalyzed reactions, such as in the unusual *methylene*-selective C−H chlorination we have recently reported.[26] Interestingly, Figure 10 indicates that water oxidation could become accessible at pH 3. That reaction is currently under investigation.

As shown in Figure 2, ClO_2 is generated in an initial fast reaction upon mixing solutions of ClO_2^- with the catalysts MnTDMImP

Scheme 3. Mechanism of ClO_2^- Dismutation by MnTDMImP[a]

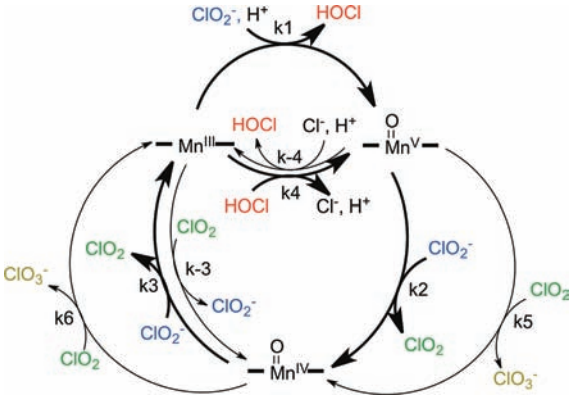

[a] The bold arrows indicate high-flux pathways. Because of the pH range of this study (4.7−6.8), hypochlorite is written in protonated form.

and MnTM23PyPz. The ClO_2 concentration was observed to rise quickly to a plateau and then to decrease with minimal catalyst bleaching in a slower subsequent phase of the reaction.

To account for the further decay of ClO_2 during the slower second phase of this catalysis, the reactions of ClO_2 with authentic oxoMn^V, oxoMn^{IV}, and Mn^{III}TDMImP were examined. Traditional stopped-flow spectroscopy indicated 1-electron redox chemistry between ClO_2 and both oxoMn^V and oxoMn^{IV} (Figure 9) to produce ClO_3^-. Indeed, chlorate ion was detected as a product by indirect ion chromatography HPLC (Table 2). Chlorine dioxide also decomposed in the presence of aquahydroxoMn^{III}TDMImP at pH 6.8 (Figure 8). The Mn^{IV}/Mn^{III} redox potential could be observed by square wave voltammetry to be 1.03 V at this pH. Thus, the reduction potential for oxoMn^{IV}/Mn^{III}TDMImP is either equal to or slightly less than that of ClO_2/ClO_2^- in the vicinity of pH 6.8, confirming that ClO_2 should be capable of oxidizing Mn^{III}. Of course, this is the reverse reaction of the observed oxidation of ClO_2^- by oxoMn^{IV} (Scheme 2, reaction 2), and we conclude therefore that this step is reversible during catalysis near neutral pH.

By accounting for the new results described here, we propose a more complete mechanism of this manganese porphyrin-chlorite reaction as shown in Scheme 3. All but two of the elementary steps of this catalytic cycle have been observed and analyzed directly by stopped-flow methods. The endergonic oxidation of Mn^{III} by ClO_2^- is the rate-limiting step for this system (k_1) and cannot be directly observed because of the rapid subsequent steps. Similarly, the oxidation of Mn^{III} to oxoMn^{IV} by ClO_2 (k_{-3}) could not be directly observed, as the reverse reaction (reduction of oxoMn^{IV} by ClO_2^-) is shown to progress fully under the conditions studied.

Although we could not directly observe the 2-electron oxidation of Mn^{III} by ClO_2^-, the rate constant of this step was inferred by monitoring the first-order decay of ClO_2^- ion during turnover. A steady-state approximation (Supporting Information) f or the mechanism in Scheme 1 suggests that the rate constant (k_{app}) for ClO_2^- consumption is equal to 5 k_1 [Mn^{III}], where k_1 is the apparent second-order rate constant for oxo-transfer from ClO_2^- to Mn^{III}. Indeed, at pH 6.8 the first-order conversion of ClO_2^- by 8.6 μM MnTDMImP is constant ($(2.92 \pm 0.19) \times 10^{-3}$ s^{-1}) and predicts a k_1 equal to 68 ± 4.4 M^{-1} s^{-1}. This value is consistent with an initial rate analysis of the same data (Supporting Information).

Kinetic Simulation of the Mechanism. To evaluate the proposed scheme (and the reversibility of oxoMn^{IV} reduction by ClO_2^-), the mechanism in Scheme 3 was modeled by kinetic simulation. Experimentally determined rate constants for all known reactions were used, (Table 4) and the model was fitted to ClO_2 growth and decay curves such as those in Figure 3 and Figure 8. The rate constant k_{-3}, corresponding to the oxidation of Mn^{III} by ClO_2 was left as an unconstrained parameter. Two computational fits of the model to the data provided calculated k_{-3} values of 3.04×10^2 or 6.64×10^2 M^{-1} s^{-1} (Figure 11). The predicted k_{-3} value (when taken with the experimentally observed k_3) allows calculation of a K_{eq} to be ~7.5, in agreement with our prediction of a reversible step near pH 6.8. The Mn^{IV}/Mn^{III} reduction potential that can be calculated from these equilibrium values is between +1.0 V and +1.13 V, depending upon which of several standards is used for the oxidation potential of chlorite ion,[27] essentially the same as the measured value (1.03 V) and those reported for other cationic manganese porphyrins.[28−30] Thus, the Mn^{IV}/Mn^{III} reduction potential of MnTDMImP is well matched to that of chlorite ion such that Mn^{IV} does not accumulate during catalysis.

Activation Parameters for Oxo-transfer from ClO_2^- to Mn(III)TDMImP. Using the data from Figure 3, it was possible to extract second-order rate constants for the oxidation of Mn^{III} by ClO_2^- at pH 6.8 over the temperature range 5−35 °C (Supporting Information, Figure S3a). Using these values, thermodynamic activation parameters could be determined for the initial oxo-transfer reaction; $\Delta H^{\ddagger} = +44.4$ kJ mol^{-1} and $\Delta S^{\ddagger} = -60.7$ J mol^{-1} K^{-1}.

Positive, moderate $\Delta H^{\ddagger}$ values and negative $\Delta S^{\ddagger}$ values have been associated with heterolytic O−O bond cleavage of iron,[31] chromium,[32] and manganese peroxides,[12] leading to metal-oxo formation. The calculated $\Delta H^{\ddagger}$ value is similar to that reported for oxygen atom transfers to phosphites and phosphonites from dioxomolybdenum and dioxotungsten complexes (+34 to +58 kJ mol^{-1}).[33] Heterolysis of the O−Cl bond in a chloritomanganese(III) adduct leading to oxoMn^V would be analogous to the concerted and entropically unfavorable O−O cleavage in HOO-Mn^{III}TDMImP (Scheme 4).[12] A negative activation entropy term would also arise from the bimolecular nature of the proposed manganese porphyrin oxidation by chlorite ion. Another similarity between these two heterolytic reactions is the pH independence that is observed, suggesting a similar push−pull protonation−deprotonation scenario in both mechanisms.

Chlorite as a 1- or 2-Electron Oxidant. The kinetic data reported here argues that ClO_2^- reacts with Mn^{III} via oxo-transfer to generate dioxoMn^{V}TDMImP and HOCl. Further, the observed steady-state equilibrium shown in Figure 6 shows that HOCl does not reduce dioxoMn^{V}TDMImP at a detectable rate. Another conceivable pathway from an initial chloritomanganese(III) adduct would lead via Cl−O bond homolysis to an oxo-Mn^{IV} intermediate and chloroxy radical (ClO$^{\bullet}$), as suggested by Abu-Omar et al.[9] A similar homolysis mechanism has been implicated computationally for chloritoiron(III) porphyrins.[34] Chlorite is known to act as both a 1- and 2-electron oxidant with transition metal systems.[35] As discussed above, the rationale for our proposal of ClO_2^- as a 2-electron oxidant is the similar ΔG° for oxo-transfer from both ClO_2^- and hypobromite (BrO^-),[20] the latter a known oxo-transfer reagent in manganese porphyrin chemistry. Further, ClO_2^- has been demonstrated to be an

dx.doi.org/10.1021/ic201430v |Inorg. Chem. 2011, 50, 10353–10362

Table 4. Collected Apparent Second-Order Rate Constants for the Elementary Steps in the Decomposition of ClO_2^- by MnTDMImP[a]

		k_{app} (M^{-1} s^{-1})	
	reaction	pH 4.7	pH 6.8
k_1	$Mn^{III} + ClO_2^- \rightarrow oxoMn^V + ClO^-$	$(2.50 \pm 0.13) \times 10^2$	$(6.80 \pm 0.14) \times 10^1$
k_2	$oxoMn^V + ClO_2^- \rightarrow oxoMn^{IV} + ClO_2$	$(6.77 \pm 0.08) \times 10^5$	$(6.30 \pm 0.62) \times 10^3$
k_3	$oxoMn^{IV} + ClO_2^- \rightarrow Mn^{III} + ClO_2$	$(6.03 \pm 0.06) \times 10^3$	$(3.13 \pm 0.12) \times 10^3$
k_{-3}	$Mn^{III} + ClO_2 \rightarrow oxoMn^{IV} + ClO_2^-$	n.d.	$(4.59 \pm 2.37) \times 10^{2b}$
k_4	$Mn^{III} + ClO^- \rightarrow oxoMn^V + Cl^-$	$(6.64 \pm 0.23) \times 10^4$	$(1.71 \pm 0.27) \times 10^6$
k_{-4}	$oxoMn^V + Cl^- \rightarrow Mn^{III} + ClO^-$	1.30×10^{7c}	1.42×10^{2c}
k_5	$oxoMn^V + ClO_2 \rightarrow oxoMn^{IV} + ClO_3^-$	$(2.24 \pm 0.14) \times 10^4$	$(1.61 \pm 0.12) \times 10^4$
k_6	$oxoMn^{IV} + ClO_2 \rightarrow Mn^{III} + ClO_3^-$	$(7.90 \pm 0.53) \times 10^3$	$(1.19 \pm 0.06) \times 10^4$

[a] All errors represent standard errors of linear fit analyses as described in the text; For simplicity, both HOCl and ClO^- are represented in reactions 1, 4, and −4 as ClO^-; n.d, not determined. [b] k_{-3} reported as the average of two values determined from computational fit of mechanism to data (see text); [c] k_{-4} calculated from measured k_4 and K_{eq};

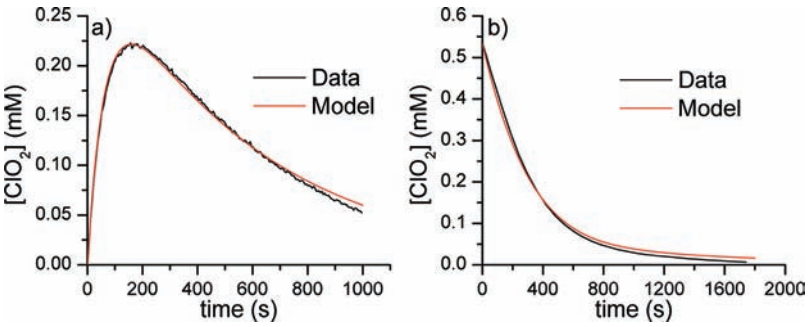

Figure 11. Modeling data for the mechanism in Scheme 3. Empirically determined rate constants were used for all steps except $Mn^{III} + ClO_2$ (k_{-3}). The kinetic simulations varied parameter k_{-3} to determine the best fit of data. (a) Data from Figure 3, 25 °C. Model calculates $k_{-3} = 6.64 \times 10^2$ M^{-1} s^{-1}. (b) Data from Figure 8. Model calculates $k_{-3} = 3.04 \times 10^2$ M^{-1} s^{-1}.

Scheme 4. Proposed Mechanism for pH-Independent O-X Heterolysis for the Formation of *trans*-Dioxomanganese(V)

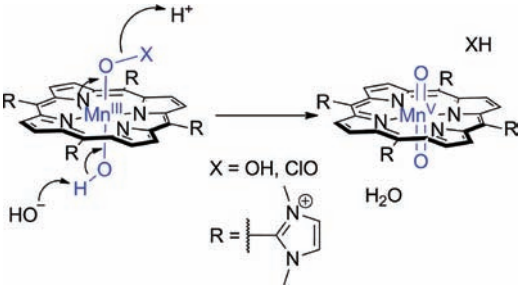

oxo-transfer "shunt" oxidant for manganese porphyrins in organic solvents, generating presumed $oxoMn^V$ intermediates.[17] Substrate oxygenations and oxygen production were reported in that case.

One can consider the two proposed oxidations of Mn^{III} by ClO_2^- as competing homolysis and heterolysis of the O−Cl bond in an inferred chloritomanganese(III) adduct (Figure 12). A chloritoiron(III) complex has been detected in an iron-catalyzed oxidation of chlorite ion at very low pH.[27] Although both of these plausible reactions are endergonic for Mn^{III}TDMImP, thermochemical considerations show that the formation of $oxoMn^V$ over $oxoMn^{IV}$ is favored by ∼25 kJ mol^{-1} at pH 6.8.

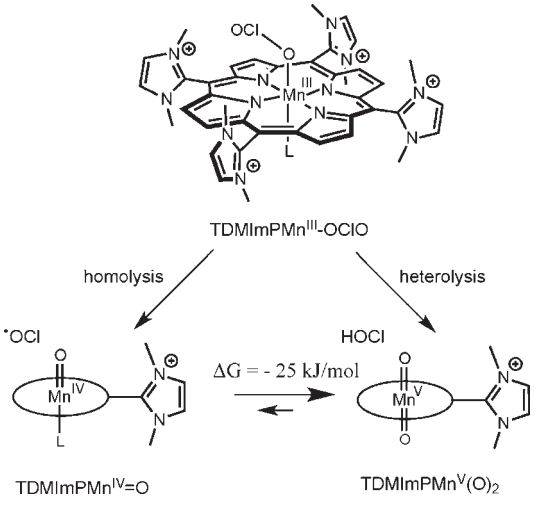

Figure 12. Hypothetical equilibrium between $oxoMn^{IV}$ and $oxoMn^V$ as a result of heterolytic or homolytic cleavage of the O−Cl bond from a chloritomanganese(III) adduct.

While we have not directly measured the redox potential for *trans*-dioxoMn^VTDMImP/oxoMn^{IV}TDMImP, this value can be determined using the thermodynamics of other measured reactions. The redox potential for the two-electron reduction of

trans-dioxoMn^{V}TDMImP to give Mn^{III}TDMImP has been previously determined to be $E'_{Mn(V)/Mn(III)}$ = +1.13 V vs NHE.[13] The redox potential for the one-electron reduction of oxomanganese(IV) to give manganese(III) was measured electrochemically to be $E'_{Mn(IV)/Mn(III)}$ = +1.03 V vs NHE for this porphyrin at pH 6.8. From these two values ($E'_{Mn(V)/Mn(III)}$ and $E'_{Mn(IV)/Mn(III)}$), the reduction potential for the couple oxoMn^{V}/oxoMn^{IV} can be determined to be $E'_{Mn(V)/Mn(IV)}$ = +1.23 V at this pH (Supporting Information). Given the very high oxidation potential for hypochlorous acid ($E°(ClO^{•}/ClOH)$ = +1.86 V vs NHE),[36] the *heterolytic* oxygen atom transfer from chlorite ion in Figure 12 appears to be strongly favored for Mn^{III}TDMImP.

SUMMARY AND CONCLUSIONS

We have investigated the mechanism of a manganese porphyrin-catalyzed chlorine dioxide production from chlorite ion. This process involves rate-limiting oxidation of the manganese(III) catalyst by ClO_2^- to afford high-valent manganese species. We argue on kinetic, electrochemical, and thermodynamic grounds that this initial intermediate is the same *trans*-dioxoMn^{V}TDMImP species that we have previously observed in reactions of this manganese porphyrin with hypobromite[13] and hydrogen peroxide.[12] Both oxoMn^{V} and oxoMn^{IV} oxidize ClO_2^- directly to ClO_2. Interestingly, both the oxidation of ClO_2^- by oxoMn^{IV} and the oxo-transfer from HOCl to Mn^{III} were found to be fast and reversible near pH 6.8. The ClO_2 evolved from this catalysis is itself further oxidized to ClO_3^- by oxoMn^{V} and oxoMn^{IV} in a slower subsequent phase of the reaction. The entire catalytic process can be modeled via kinetic simulation, in very good agreement with empirical ClO_2 growth and decay curves and the measured ClO_3^- that is produced.

The fast and efficient evolution of ClO_2 catalyzed by MnTDMImP and MnTM23PyPz suggest that a viable, scalable, and acid-free process could be developed for chlorine dioxide production using these catalysts. As we have previously demonstrated, the evolved ClO_2 can be efficiently removed from the reaction vessel via simple sparging or air stripping during turnover. Further, the catalysts are active on a solid support, suggesting their use in a flow system, a cartridge, or a trickle-bed reactor.[8] The mechanism of this catalytic process now suggests methods for greatly enhancing the rate of ClO_2-generation under mild, neutral conditions. Efforts to address the practical implementation of manganese porphyrin-generated ClO_2 are under way.

EXPERIMENTAL SECTION

Reagents. Sodium chloride, sodium chlorate, *t*-butyl hydroperoxide (70% aqueous solution), and Oxone were purchased from Aldrich and used as received. Sodium chlorite was obtained from Aldrich as >80% technical grade and recrystallized twice from ethanol/water (>95% final). All oxidant stock solutions were prepared fresh daily and standardized by iodometric titration before use. Dilute (0.5−10.0 mM) chlorite solutions were standardized spectrophotometrically ($\varepsilon_{260\ nm}$ = 154 cm^{-1} M^{-1}).[15] Buffers were prepared fresh each day using either acetic acid/sodium acetate (pH = 4.7, 5.7) or potassium phosphate (monobasic)/potassium phosphate (dibasic) (pH = 6.8, 8.0) and pH-adjusting no more than 0.1 units using perchloric acid or sodium hydroxide. ClO_2 was prepared from ClO_2^- using a previously reported procedure.[37] Briefly, a 2.5% w/w solution of $NaClO_2$ was acidified with sulfuric acid under an argon flow in the dark. The evolved gas was carried by the argon flow through a gas scrubbing tower containing a 2.5% w/w solution of $NaClO_2$ and bubbled through deionized water in a chilled amber bottle. Aliquots of the resulting solution were frozen at −30 °C for prolonged storage. The concentration of ClO_2 was checked immediately prior to use ($\varepsilon_{359\ nm}$ = 1230 cm^{-1} M^{-1}).[15] Leftover ClO_2 from all experiments was neutralized with sodium iodide before being disposed of in general waste. Mn^{III}TDMImP was synthesized as the chloride salt using reported procedures,[13] and MnTDMBImP was prepared analogously from *N*-methyl-2-benzimididazole-carboxaldehyde. MnTM2PyP and MnTM4PyP were purchased from Mid Century and purified by double precipitation. MnTM23PyPz was prepared following the method of Wöhrle et al.[38] Briefly, manganese diacetate (170 mg) and pyridine-2,3-dicarbonitrile (500 mg) were heated in an unsealed reaction tube to 200 °C with mechanical stirring for 4 h. The deep blue solid product (a mixture of isomers) was washed with acetone, isolated by filtration, suspended in 50 mL of dimethylformamide (DMF), and tetra-methylated using excess dimethyl sulfate at 120 °C for 12 h. The product was precipitated with acetone and purified by double precipitation.

Instrumentation. UV−vis spectroscopic measurements were taken using a Hewlett-Packard 8453 diode array spectrophotometer equipped with a temperature-controlled cell housing, VWR 1140 thermostat bath and a Hi-Tech SFA Rapid Kinetics Accessory. Stopped-flow experiments for fast reactions were carried out using a Hi-Tech SF-61 double-mixing instrument with a 1 cm path length equipped with an ISOTEMP 1016 S thermostat bath. Ion chromatography was accomplished with an HPLC system consisting of a Waters 600 controller, Hamilton PRP X-100 column, and Waters 996 photodiode array detector.

Stopped-Flow Experiments. Reactions of ClO_2^- with Mn^{III} porphyrins were studied using traditional UV−vis and rapid mixing techniques.[39] Solutions of catalyst and ClO_2^- were prepared in buffered solutions and mixed 1:1. All rate calculations were based on final concentrations resulting from this dilution. The oxidations of ClO_2^- and ClO_2 by oxoMn^{V}TDMImP and oxoMn^{IV}TDMImP were studied in double mixing mode using diode array detection. Solutions of Mn^{III}TDMImP and oxidant (oxone, tBuOOH) were prepared in weak pH = 8.0 phosphate buffer (10 mM) and mixed 1:1 in a first push. After a short aging time to ensure complete conversion to the high-valent species (2−150 s, fine-tuned for each experiment), the porphyrin solution was mixed 1:1 with the substrate (ClO_2^- or ClO_2) prepared in a higher strength buffer (100 mM) at the pH to be studied (4.7 or 6.8). All concentrations used in subsequent rate calculations accounted for the 4-fold and 2-fold dilutions inherent to the double-mixing technique. Each reaction was run in duplicate or triplicate at T = 25 °C, and most errors in measured rate constants were < ± 2.0%. In many cases in the text, the error bars in the reported data are smaller than the data point marker. Averaging of the runs and analysis of the data was accomplished using the KinetAsyst 3 software package. Kinetic simulations of the overall mechanism were performed with the Berkeley-Madonna software package.

Ion Chromatography Experiments. Aliquots of ClO_2^- or ClO_2 solutions were added to buffered solutions of Mn^{III}TDMImP under mechanical stirring at ambient temperatures. ClO_3^- was quantified using an indirect ion chromatography method.[16] In brief, an aqueous solution of 4-aminosalicylic acid (4 mM) was pH adjusted to pH = 6.0 and employed as the mobile phase. Reaction samples were injected directly without any modification. The eluent was monitored at 320 nm, and a decrease in absorbance was observed as anions were eluted. Concentration of analyte was calculated directly from total area of the peak using a concentration curve prepared daily using prepared standards.

Temperature-Dependence on ClO_2 Evolution. Buffered solutions (100 mM) of Mn^{III}TDMImP and ClO_2^- were mixed 1:1 and monitored in the UV−vis. The cell holder and mixing accessory were equilibrated to the set temperature for 30 min before the measurement.

■ ASSOCIATED CONTENT

Supporting Information. Ionic strength and pH rate plots, temperature effect and Arrhenius plot, derivation of kinetics and Nernst equations, initial rate analysis. This material is available free of charge via the Internet at http://pubs.acs.org.

■ AUTHOR INFORMATION

Corresponding Author
*Phone: (609) 258-3593. Fax: (609) 258-0348. E-mail: jtgroves@princeton.edu.

■ ACKNOWLEDGMENT

We are grateful for support of this research by the National Science Foundation (CHE 0616633). We thank Christina Chang for technical assistance.

■ REFERENCES

(1) Gordon, G.; Rosenblatt, A. A. *Ozone: Sci. Eng.* **2005**, *27*, 203.
(2) *White's Handbook of Chlorination and Alternative Disinfectants*, 5th ed.; Wiley: New York, 2010.
(3) Canter, D. A.; Gunning, D.; Rodgers, P.; O'Connor, L.; Traunero, C.; Kempter, C. J. *Biosecurity and Bioterrorism-Biodefense Strategy Practice and Science* **2005**, *3*, 119.
(4) Lee, H. K.; Deshwal, B. R. *J. Ind. Eng. Chem.* **2005**, *11*, 330.
(5) Tarvo, V.; Lehtimaa, T.; Kuitunen, S.; Alopaeus, V.; Vuorinen, T.; Aittamaa, J. *Ind. Eng. Chem. Res.* **2009**, *48*, 6280.
(6) Huang, J. L.; Cheng, L. H.; Zhao, Z. Y. *Water Res.* **2001**, *35*, 2570.
(7) Anastas, P. T.; Warner, J. C. *Green Chemistry: Theory and Practice*; Oxford University Press: New York, 1998.
(8) Umile, T. P.; Groves, J. T. *Angew. Chem., Int. Ed.* **2011**, *50*, 695.
(9) Hicks, S. D.; Petersen, J. L.; Bougher, C. J.; Abu-Omar, M. M. *Angew. Chem., Int. Ed.* **2011**, *50*, 699.
(10) Lee, A. Q.; Streit, B. R.; Zdilla, M. J.; Abu-Omar, M. M.; DuBois, J. L. *Proc. Natl. Acad. Sci. U.S.A.* **2008**, *105*, 15654.
(11) Zdilla, M. J.; Lee, A. Q.; Abu-Omar, M. M. *Inorg. Chem.* **2009**, *48*, 2260.
(12) Jin, N.; Lahaye, D. E.; Groves, J. T. *Inorg. Chem.* **2010**, *49*, 11516.
(13) Lahaye, D. E.; Groves, J. T. *J. Inorg. Biochem.* **2007**, *101*, 1786.
(14) Jin, N.; Ibrahim, M.; Spiro, T. G.; Groves, J. T. *J. Am. Chem. Soc.* **2007**, *129*, 12416.
(15) Furman, C. S.; Margerum, D. W. *Inorg. Chem.* **1998**, *37*, 4321.
(16) Mehra, M. C.; Pelletier, C. *Chromatographia* **1990**, *30*, 337.
(17) Slaughter, L. M.; Collman, J. P.; Eberspacher, T. A.; Brauman, J. I. *Inorg. Chem.* **2004**, *43*, 5198.
(18) Jakopitsch, C.; Spalteholz, H.; Furtmuller, P. G.; Arnhold, J.; Obinger, C. *J. Inorg. Biochem.* **2008**, *102*, 293.
(19) Shahangian, S.; Hager, L. P. *J. Biol. Chem.* **1981**, *256*, 6034.
(20) Holm, R. H.; Donahue, J. P. *Polyhedron* **1993**, *12*, 571.
(21) Lieb, D.; Zahl, A.; Shubina, T. E.; Ivanović-Burmazović, I. *J. Am. Chem. Soc.* **2010**, *132*, 7282.
(22) Jin, N.; Groves, J. T. *J. Am. Chem. Soc.* **1999**, *121*, 2923.
(23) De Angelis, F.; Jin, N.; Car, R.; Groves, J. T. *Inorg. Chem.* **2006**, *45*, 4268.
(24) Bratsch, S. G. *J. Phys. Chem. Ref. Data* **1989**, *18*, 1.
(25) Jin, N.; Bourassa, J. L.; Tizio, S. C.; Groves, J. T. *Angew. Chem., Int. Ed.* **2000**, *39*, 3849.
(26) Liu, W.; Groves, J. T. *J. Am. Chem. Soc.* **2010**, *132*, 12847.
(27) Fabian, I.; Gordon, G. *Inorg. Chem.* **1992**, *31*, 2144.
(28) Chen, F.-C.; Cheng, S.-H.; Yu, C.-H.; Liu, M.-H.; Su, Y. O. *J. Electroanal. Chem.* **1999**, *474*, 52.
(29) Weitner, T.; Budimir, A.; Kos, I.; Batinic-Haberle, I.; Birus, M. *J. Chem. Soc., Dalton Trans.* **2010**, *39*, 11568.
(30) Budimir, A.; Smuc, T.; Weitner, T.; Batinic-Haberle, I.; Birus, M. *J. Coord. Chem.* **2010**, *63*, 2750.
(31) Groves, J. T.; Watanabe, Y. *J, Am. Chem. Soc.* **1988**, *110*, 8443.
(32) Pestovsky, O.; Bakac, A. *J. Chem. Soc., Dalton Trans.* **2005**, 556.
(33) Tucci, G. C.; Donahue, J. P.; Holm, R. H. *Inorg. Chem.* **1998**, *37*, 1602.
(34) Keith, J. M.; Abu-Omar, M. M.; Hall, M. B. *Inorg. Chem.* **2011**.
(35) Fabian, I. *Coord. Chem. Rev.* **2001**, *216*, 449.
(36) Huie, R. E.; Clifton, C. L.; Neta, P. *Radiat. Phys. Chem.* **1991**, 477.
(37) Medir, M.; Giralt, F. *Water Res.* **1982**, *16*, 1379.
(38) Wöhrle, D.; Gitzel, J.; Okura, I.; Aono, S. *J. Chem. Soc., Perkin Trans. 2* **1985**, 1171.
(39) Lee, J. B.; Hunt, J. A.; Groves, J. T. *J. Am. Chem. Soc.* **1998**, *120*, 6053.